Evaluations of LIDAR reflectance amplitude sensitivity towards land cover conditions

Hiroyuki HASEGAWA

Abstract

This study aims to investigate the characteristics of LIDAR intensity data for executing land cover classification. The quantitative and qualitative analysis was executed with reflection geometry model and land cover classification data. By these analyses, the LIDAR intensity feasibility for classification was discussed. The survey found that intensity is inversely proportional to angle and distance, though their relation did not agree with the theoretical model. The survey also found that intensity correction with distance and angle is not always applicable, the effect of correction is not significant, and consequently raw intensity value usage is justified. We conclude that some land cover and building materials were separable with intensity data. Old asphalt and grass were separable though cement, slate & zinc, brick, and trees were not easy to recognize. Soil, gravel, and grass could be distinguishable each other.

1. Introduction

This study aims to investigate the characteristics of LIDAR intensity data for executing land cover classification. The quantitative and qualitative analysis was executed with a reflection geometry model and land cover classification data. By these analyses, the LIDAR intensity feasibility for classification was discussed.

Hug (1996) discussed methods to acquire LIDAR intensity and showed some combinations of elevation data with intensity data. They concluded that intensity data added supplemental information and that it is useful for feature extraction.

Song et al. (2002) applied filters to a grid intensity data and evaluated their potential. They also classified asphalt, grass, roof, and trees with intensity data. They concluded that though the observed intensities did not agree with the theoretical ones, the relative value is reliable and intensity is functional for classification.

Lutz et al. (2003) investigated the LIDAR intensity characteristics of each land class (in a glacial area). They also made a reflection model from distance, elevation, and a reflection geometry model and then inquired into the effect of each factor. They found that laser range, surface elevation, and surface class affected to the LIDAR intensity in that order. They also pointed out that intensity correction with distance is inadequate because intensity varied with elevation and surface class.

This study was applied to the ground survey and aerial survey for investigating the characteristics of LIDAR intensity data. In the ground survey, a laser scanner detached from a helicopter was set on the ground, laser pulses irradiated targets of different materials, and the intensity was measured under various conditions (distance and angle). We checked the angle and distance dependency of the laser intensity. We also checked whether observed data follow a reflection model and discussed the intensity characteristics of land cover materials.

In the aerial survey, we examined the angle and distance dependency and the adaptability of the reflection model. We also examined the efficiency of intensity correction with angle and distance. Finally we described the intensity characteristics of each land cover class and the possibility of land cover classification.

2. Reflection model

When light illuminates an object, three types of reflection are observed. They are diffuse reflection light, specular reflection light, and ambient light.

Ambient light is not the light directly reflected by the target but the light scattered by air dust or surrounding objects. It comes from every direction and its intensity is constant everywhere.

Diffuse reflection light is the light reflected on a tarnished surface. Its intensity is almost constant regardless of incident angle and follows the Lambert's cosine law (Aytaç and Barshan, 2005). According to the law, the intensity of diffuse reflection light is proportional to the angle between the angle of incidence and the surface normal. Furthermore, the intensity is inversely proportional to the distance between the target and the observation point. As a result, the diffuse reflection light (I_d) is:

$$I_d = R_d * \cos(\theta)/x^2 \tag{1}$$

where x is distance between the target and the observation point, θ is the angle between the incident direction and the surface normal, and R_d is the diffuse reflection coefficient.

Specular reflection light is the light reflecting on a mirror-like surface. On these surfaces, the light strongly reflects in a specific direction and the intensity rapidly decreases as the angle deviation widens. Additionally, the specular reflection coefficient is generally a function of the incident angle and different materials have different coefficients. As a result, the specular reflection light (I_S) is:

$$I_s = W(\theta) * \cos^n(\gamma)/x^2 \tag{2}$$

where the θ is the angle of incidence, W is the specular reflection coefficient function, and γ is the angle between the angle of reflection and the angle of observation. The exponent *n* determines the sharpness of the specular light. *n* is typically between 1 and 200.

In the LIDAR survey, the angle of incidence and the angle of observation are the same. Furthermore, supposing that the specular reflection coefficient is constant, the equation above can be written:

$$I_s = W * \cos^n(2\theta)/x^2 \tag{3}$$

where W is the specular reflection coefficient.

The Phong illumination model, which is commonly used for the light formulation, describes the light intensity with 3 types of reflection. As the ambient light is negligible in the LIDAR survey, the observed light (I_r) is the sum of the diffuse reflection light and the specular reflection light, and the reflection model can be written:

$$I_r = I_d + I_s = R_d \cos(\theta)/x^2 + W \cos^n(2\theta)/x^2 \tag{4}$$

3. Methods

3.1 On the ground experiments

On the ground experiments were done on 9 March 2004 and 12 March 2004. They ware conducted with a laser scanner detached from an airborne LIDAR system. The scanner was fixed on the ground and connected to a constant potential dynamo.

The targets were made from lath boards 1m square. They were reinforced with a wooden frame. Materials were glued to the target. Eight materials were selected; new asphalt, old asphalt, soil, gravel, grass, cement, bricks, and roof tiles. The targets were attached to a holder (Fig. 1). There is a protractor beside the target and we can easily set it at a proper angle.

Fig. 1 Equipment for on the ground survey. The brick target (top left) and the holder with the target (top right). The target is 1m square. The holder has protractors on both sides (bottom left). Looking at the target from near the laser scanner (top right).

The scan angle of the scanner was fixed to 0 degrees and the beam divergence angle was 0.5 mrad, which corresponds to a 5 cm footprint at a distance of 100 m.

The range dependency trend was measured at five distances; 60 m, 65 m, 70 m, 75 m, and 80 m. Benchmark point was determined for each distance and the holder rim was set to match the point.

Angle dependency trend was measured between 0° and 45° in increments of 5° at a fixed distance of 70 m. The protractors, which were attached both sides of the holder, determined the angle.

The measurement period was 10 minutes

(corresponding to 200,000 pulses) for each condition, and both distance and intensity were obtained.

Table 1 Specification of aerial LIDAR survey.

Study Area Characteristics	
Location	Central Tsukuba
Area	1.7km^2
Flight Characteristics	
Flight Date	19 Feb, 2005
Flight Altitude	1500m
Flight Speed	180kt
Number of Courses	4 courses (parallel)
Scan Characteristics	
LIDAR system	ALTM2050DC
Pulse Rate	50kHz
Scan Frequency	50Hz
Scan Angle	±8°
Side lap	40%

3.2 Aerial observations

Aerial observation was carried out on 12 Feb 2005. General information on the flight is summarized in Table 1. The study area is located in Tsukuba city, Japan, and contains some large buildings, housing complexes, and detached houses sparsely spreading in farmlands.

The positions and altitudes of the scanner where the pulse was shot were calculated from GPS/IMU data. Then the positions of reflection were computed.

Ground points were sieved out from height object points. Then, DTM, DSM, and DIM (Digital Intensity Model) were generated in both random point format and grid format. Grid DIM value indicates intensity of laser points that belonged to a height object and have maximum value in a grid.

4. Result and discussion

4.1 On the ground experiments

4.1.1 Raw intensity profile

Fig. 2 shows the raw intensity profile of cement and brick. In the above profile, the measured intensity is stable. In the bottom profile, however, the intensity fluctuates more widely, especially at the beginning of measurement. To obtain more reliable statistical values, the measured values of the first 1 second were cut off. Additionally, points were omitted if the variance of the point exceeded 3σ

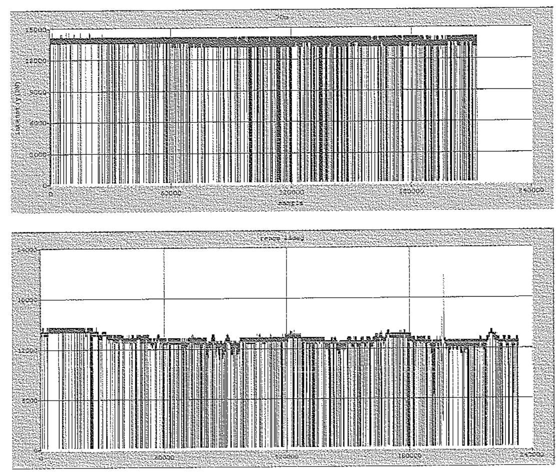

Fig. 2 Raw profile of cement (above) and brick (Below)

4.1.2 Distance dependency

Fig. 3 shows the distance dependency test result. Intensity value declines with an increase of distance except for a distance of 70m. We verify the suitability of the reflection model with the obtained result. If the incident angle equals 0°, the model can be described as follows;

$$I_r = a/x^2 \tag{5}$$

Equation (5) was fit to the field data by the nonlinear least-square (NLLS) method. The fit command of Gnuplot was used for fitting. Gnuplot uses the Marquardt-Levenberg algorithm for NLLS (Williams and Kelly, 2004). The data observed at the distance of 70m was not used during the calculation because the data seemed to be abnormal. The adjusted parameter was a = 5.266992e+07 ± 2.204e+06. The estimated intensity from the model is shown in Fig. 3 by a red line. The resultant value of reduced chi-square was 8.45929 and the number of degrees of freedom (NDF) was 3. The probability of the chi-square distribution was 1.29e-05. This value demonstrates that the model is inadequate for the observed result.

The obtained intensity data seems to have an inverse relation to the distance. Thus, we inspected whether the data follows the formula:

$$I_r = a/x^n \tag{6}$$

The fitting result is that a = 64500 ± 2430, n = 0.85241 ± 0.0205, the reduced chi-square is 0.00951682, and NDF is 2. These values indicate that the data are inversely proportional to the distance rather than its square.

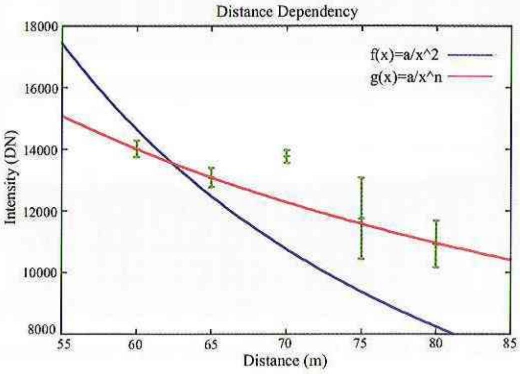

Fig. 3 Distance dependency of intensity. Vertical bar shows standard deviation. Red line indicates the regression line.

4.1.3 Angle Dependency

Fig. 4 shows the angle dependency experiment result. The distance between the scanner and the target was fixed at 70m. In soil, cement, roof tile, and old asphalt, intensity decreases as incident angle increases. In brick, grass, and new asphalt, however, intensity is almost constant regardless of angle. For gravel, a trend was unclear.

We verified the suitability of the reflection model. In this test series, the incident angle and reflection angle are the same. Moreover, the distance is constant. Therefore, we can rewrite equation 4 as

$$I_r = a * \cos(\theta) + b * \cos^n(2\theta) \tag{7}$$

where θ represents incident angle.

It was hypothesized that the survey results can be explained by equation 7, and this hypothesis was verified by the chi-square test for each target. Some suspicious values were not used for the regression. When the critical region was set to 5%, grass and brick were accepted. In both cases, however, the specular reflection factor was less than zero. Thus, we tested the reflection model without the specular reflection (this means b is fixed to zero), and it was found that only brick was accepted. Furthermore, if the critical region was set to 1%, soil was also accepted. Other targets were rejected or failed to fit.

The angle dependency tests revealed that LIDAR intensity will follow the reflection model in some materials but correction of intensity may be difficult.

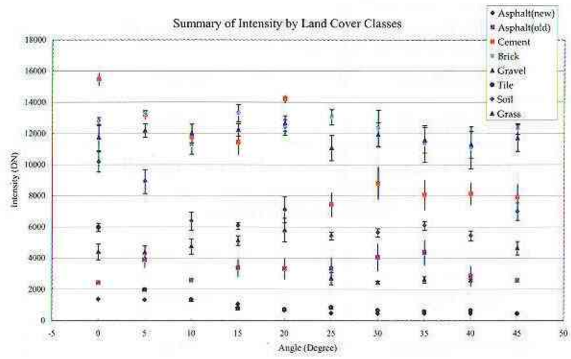

Fig. 4 Angle dependency of intensity.

4.1.4 Intensity characteristics of surface class

The scan angle was from 2° to 15° for most cases. Fig. 5 shows the calculated intensity range from 0° to 15° from angle dependency survey results.

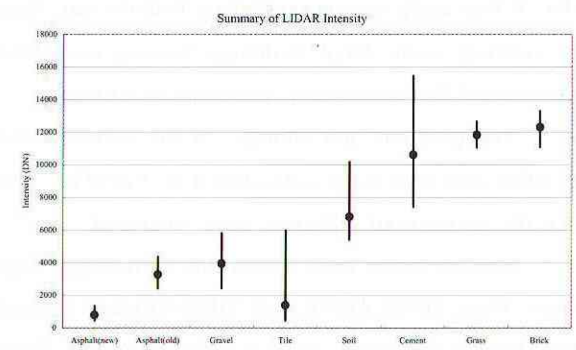

Fig. 5 Intensity characteristics of surface class. Incident angle is between 0° and 15°. Black circles indicate average intensity.

Surfaces can be grouped by their intensity. New asphalt, old asphalt, gravel, and roof tiles have lower intensity. The range of roof tiles is so wide that the other three classes were completely overlapped by it. However, roof tile can be seen only on the roofs of buildings and the others mainly lie on the ground. Thus, we can distinguish roof tiles from others if height objects are separated from the ground by DSM.

As for soil, it slightly overlaps with cement. This means that we can categorize soil area if a proper threshold for intensity is set.

Cement, brick, and grass have higher values. The intensity range of grass is quite narrow and it might be distinguishable. As brick and cement have a wider intensity range and they almost overlap each other, they might be hard to separate.

5. Aerial survey result

Fig. 6 shows the flight course and the target area. The target area was covered by four parallel courses. Another course, perpendicular to the courses, was used for integrity checking. Fig. 7 shows the obtained DIM and colour ortho image. The defect ratio was 2.1%. The ratio was the number of pixels where no return pulse was found in the pixel to the number of all pixels. At first, DIM was made course by course. Then all data was mixed and DIM that covered the whole area was made. DSM and DTM were also made in this manner. The image from a digital camera, geo-referenced by GPS/IMU, was projected to DSM of the whole area and an ortho image was created.

Fig. 6 The target area and the flight tracks. Red number indicates course no. Course 5 is only used for integrity check.

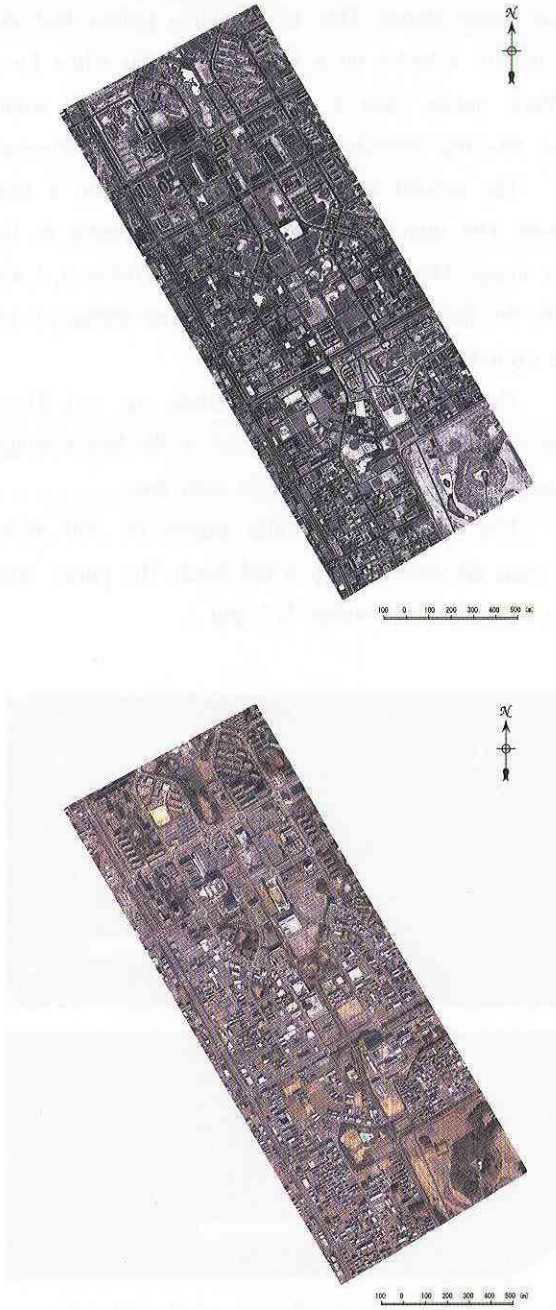

Fig. 7 DIM (top) and ortho image (bottom) of the target area.

Land cover classification data was made by a manual interpretation of a 25 cm resolution ortho image. In addition to the 8 classes described in chapter 3, 3 more classes (trees, slate or sheet zinc, and water) were added. The validity of the classification was checked with DSM and fieldwork.

For the intensity model validation test, four data sets were picked up (Fig. 8). The first set includes pulses reflected on the road. All pulses were taken in a single scan line. These pulses are indicated by the blue cross in the upper image. This set contains pulses that are reflected on vehicles, on a footbridge, or on white lines. As these pulses have a relatively high intensity, which causes incorrect statistics, they were manually eliminated.

The second set also includes pulses on a road segment. The area is indicated by a red hatch in the upper image. The pulses are taken from course 3, 4, and 6. Like the first set, pulses that have higher intensity (>15) were excluded from the calculation.

The third set includes pulses on soil. These pulses are indicated by a blue cross in the lower image. All pulses were taken in a single scan line.

The fourth set includes pulses on soil areas. The areas are indicated by a red hatch. The pulses were taken from data of courses 1, 2, and 3.

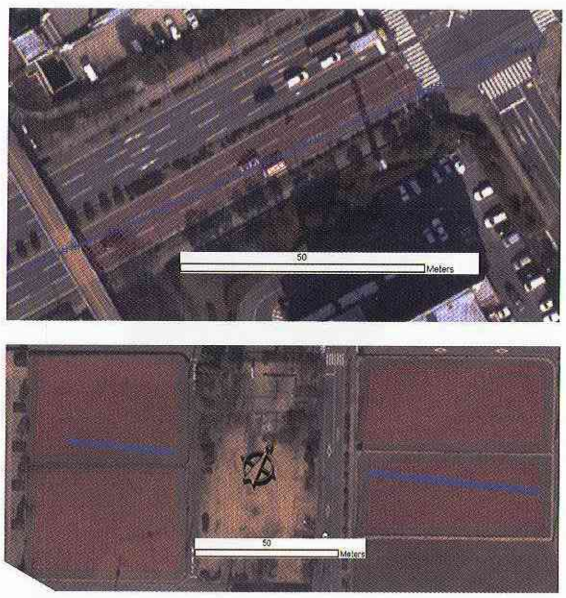

Fig. 8 Test areas of reflection model validation.

5.1 Reflection model validation

This section describes whether the reflection model is applicable to some data set and intensity correction is effective. The number of samples is more than 400 for the second and fourth set. It is known that the chi square test is unsatisfactory if the number of samples exceeds several hundred.

Fig. 9 shows the intensity of the first and second data set plotted against distance and angle. In both sets, the intensity decreases when either distance or angle increases. The reflection model was fitted to both data sets for the statistical test. The result is shown in Table 2.

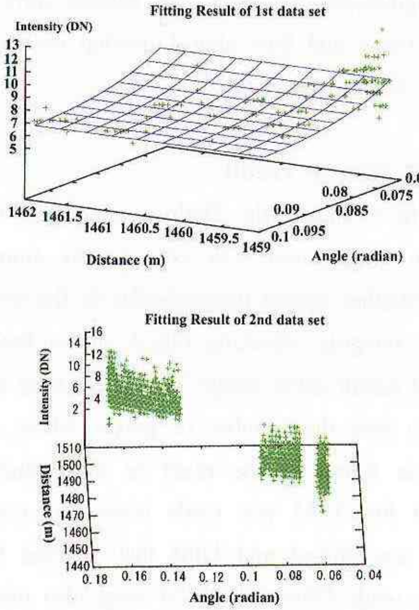

Fig. 9 Relation between intensity, distance, and angle.

Table 2 NLLS fitting results. Chi square test indicates.

data set	variable	value
1	a	-47.2728±503
	b	119.265±501.9
	m	4.88796±21.29
	χ	7.58752
	ndf	358
	RMSEA	0.14538
2	a	24.1834±54.41
	b	-7.11142±54.22
	m	39.2475±314.4
	χ	4.11878
	ndf	4726
	RMSEA	0.002946

In the first set, the test statistics (chi square value and RMSEA) indicate that the model was inadequate. In the second set, RMSEA indicates that the model was adequate. However, the coefficient of diffuse reflection was minus. Hence it follows that the model was rejected. In the third set, RMSEA was over 0.1 and the coefficient of diffuse reflection was negative, therefore the model was rejected. In the fourth set, RMSEA was over 0.1 and the coefficient of specular reflection was negative, and therefore the model was rejected. It was concluded that the applied reflection model was inappropriate for the observed data.

This segment discusses the effectiveness of intensity correction by the diffuse reflection model with range and angle. Suppose that reflection intensity is proportional to the cosine of incident angle and inversely proportional to the distance cubed, the observed value (I_0) at distance d_0 and angle θ_0 can be corrected into the adjusted value (I_c) at distance d_c and angle θ_c is:

$$I_c = I_o * \cos(\theta_c) d_o^2 / \cos(\theta_o) d_c^2 \tag{8}$$

With this equation, the observed values of each set were converted to the value at distance 1460m and angle 5°. Table 3 shows statistics from before and after the correction. The null hypothesis that there is difference amongst raw intensity and adjusted one is tested. At the significance level of 1%, T test result was rejected except for the fourth set. This means that intensity correction is ineffective in practice.

In conclusion, the model is hard to explain observed data, and intensity correction with diffuse reflection was ineffective. So using the raw intensity value for survey class characteristic calculation is appropriate.

Table 3 Statistics before and after intensity correction. T test resulted in intensity correction was only accepted at 4th data set.

data set		average	STD	range
1	raw	8.03	1.63	8.00
	adjusted	8.02	1.62	7.97
2	raw	8.12	2.03	13.00
	adjusted	8.04	2.02	13.27
3	raw	30.17	4.09	20.00
	adjusted	30.02	3.89	19.38
4	raw	29.33	3.79	28.00
	adjusted	29.15	3.76	28.38

5.2 Intensity characteristics of surface class

This section describes intensity characteristics of surface class. In the previous section, it was found that intensity correction with range and angle is difficult, therefore we use the raw value for statistics.

Based on land cover classification data, the sample areas were determined. 10 areas were selected for each class. Intensity value was picked up from DIM of each flight course. Statistics are shown in Fig. 10.

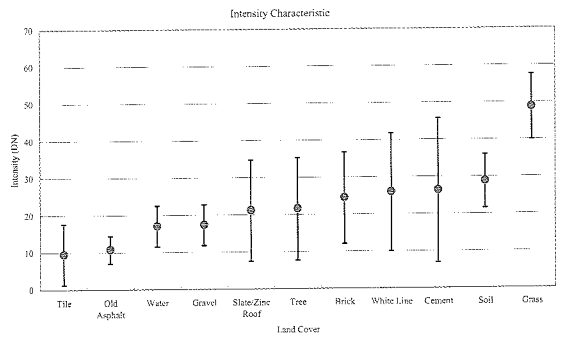

Fig. 10 Intensity characteristics of surface classes. Error bar indicates standard deviation.

Similar to the on the ground survey, the intensity of tile and old asphalt is lower in all classes. As the standard deviation of old asphalt is quite small, it is easy to distinguish from other classes. However, a white line on road has high intensity and a big standard deviation. So a recognition method of asphalt road using white lines as a clue is needed for exact extraction of roads. Because tile has different intensity from other classes that exist on roofs, it also must be easily recognized. Cement, slate & zinc, and brick, which are seen on roofs, have wide intensity variation. Additionally, there have similar intensity range. Soil, gravel, and grass mainly exist on the ground. Of these materials, gravel has relatively lower value. Grass has a higher value. Soil takes the middle value of them. These land classes have narrow standard deviation and their range does not overlap each other. This means that they can be separated from each other though cement and brick, which are other materials distributed on the ground, have spreading range and overlap with these three classes.

Trees have a wide intensity range and the range overlaps with the range of other height objects like slate & zinc, cement, and brick. This means that extraction of trees without supplementary information is difficult.

6. Conclusion

LIDAR intensity dependence on distance and angle was investigated with on the ground and aerial surveys in this paper. The on the ground survey revealed that intensity decreased in proportion to distance whereas it followed neither a traditional reflection model nor a simple diffuse reflection model. In angle dependency experiments, it was found that some materials followed the traditional reflection model, though intensity correction was difficult. An intensity characteristic survey pointed out that some land cover would be distinguished by LIDAR intensity.

An aerial survey gave the result that the reflection model was hard put to explain the observation. A simple intensity correction was not generally effective. The intensity statistics of each type of land cover pointed out that old asphalt and grass were separable, though cement, slate & zinc, brick, and trees were not easy to recognize. Soil, gravel, and grass could be distinguished from each other.

In further studies, the author will test an object extraction method with LIDAR intensity and height data for some materials. In the method, we will check out the combination of the region segmentation method with height data and classification method with intensity data.

References

T. Aytaç and B. Barshan (2005): Surface differentiation by parametric modeling of infrared intensity scans, Optical Engineering, 44(6), pp. xxx-yyy.

C. Hug (1996) Combined use of laser scanner geometry and reflectance data to identify surface objects, in: OEEPE Workshop '3-D city models', Bonn, 9-11 October, 10.

E. Lutz, Th. Geist, and J. Stötter (2003): Investigations of Airborne Laser Scanning Signal Intensity on Glacial Surfaces - Utilizing Comprehensive Laser Geometry Modelling and Orthophoto Surface Modelling (A Case Study: Svartisheibreen, Norway), Proceedings of the ISPRS Workshop on 3-D reconstruction from airborne laserscanner and INSAR data, Dresden, 143-148.

J.H. Song, S.H. Han, K. Yu, Y. Kim (2002): Assessing the Possibility of Land-cover Classification Using Lidar Intensity Data, IAPRS, 9-13 September, Graz, 34, 4.

Thomas Williams and Colin Kelley (2004): Gnuplot - An Interactive Plotting Program prepared by Dick Crawford. @ 2004/04/13 17:23:36, 163.